Physicochemical Characterization of Acrylamide/Bisacrylamide Hydrogels and Their Application for the Conservation of Easel Paintings

ARTICLE *in* LANGMUIR · FEBRUARY 2012

Impact Factor: 4.46 · DOI: 10.1021/la2044619 · Source: PubMed

7 AUTHORS, INCLUDING:

Emiliano Fratini
University of Florence
124 PUBLICATIONS **2,396** CITATIONS
SEE PROFILE

Rodorico Giorgi
University of Florence
73 PUBLICATIONS **981** CITATIONS
SEE PROFILE

David Chelazzi
University of Florence
29 PUBLICATIONS **269** CITATIONS
SEE PROFILE

Piero Baglioni
University of Florence
448 PUBLICATIONS **8,089** CITATIONS
SEE PROFILE

Langmuir

Article

pubs.acs.org/Langmuir

Physicochemical Characterization of Acrylamide/Bisacrylamide Hydrogels and Their Application for the Conservation of Easel Paintings

Giacomo Pizzorusso,[†] Emiliano Fratini,[†] Josef Eiblmeier,[†] Rodorico Giorgi,[†] David Chelazzi,[†] Aurelia Chevalier,[‡] and Piero Baglioni*[,†]

[†]Department of Chemistry and CSGI, University of Florence, via della Lastruccia 3 − 50019 Sesto Fiorentino , Florence, Italy

[‡]Aurélia Chevalier-Menu, Restauratrice du patrimoine, 289, rue Saint-Jacques 75005 Paris, France

ABSTRACT: Acrylamide chemical gels have been synthesized to obtain systems with mechanic and hydrophilic properties suitable for the cleaning of works of art. The gel characteristics were tailored by changing the polymer percentage present in the final hydrogel formulation from 2 to 10% w/w. Two different hydrogels have been selected in this interval for an in depth characterization (i.e., ***S*** 4% w/w and ***H*** 6% w/w). Water retention properties of the gels along with the free water index have been determined by the combination of standard dehydration tests and differential scanning calorimetry (DSC) measurements. The gels' structure has been determined by scanning electron microscopy (SEM) and small angle X-ray scattering (SAXS). The water retention capacity of hydrogel, *H*, was also determined. Cleaning tests on easel painting replicas, performed with both hydrogels loaded with an aqueous detergent system, showed good results in the removal of a widely used synthetic adhesive and hence offered these gels as a real alternative to the widely applied physical gel methodology with the advantage of being a residue-free technique. A preliminary SAXS investigation confirms the persistence of the detergent system nanostructure inside the hydrogel.

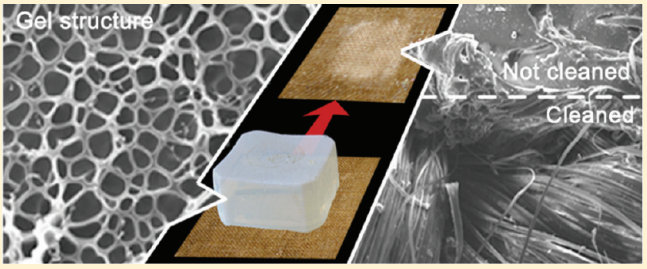

INTRODUCTION

Most of the cultural heritage exhibited in museums is constituted by easel paintings. This is a general term referred to movable works of art, painted using canvas (mainly linen and in some cases hemp), or wood as a support. All easel paintings, except for the different nature of the support, show thus a very similar stratigraphy with several layers confined in a very low thickness (less than 2−3 mm), as shown in figure 1. Natural

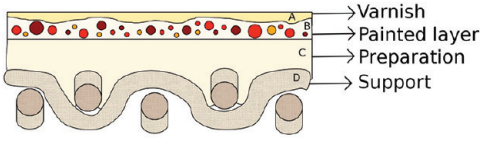

Figure 1. Schematic cross section of a typical easel painting. From top to bottom: the varnish layer (A), usually made by natural terpenic resins, ensures the protection of the painted layer and provides esthetical effects (glossiness, color saturation); the painted layer (B), constituted by mineral pigments dispersed in a binding medium (drying oil and/or egg tempera, or recently synthetic polymers); the preparation layer (C), composed by a mix of gypsum (calcium sulfate) and/or white lead (lead carbonate powder), and animal glue; the support (D), consisting of either canvas or wood.

aging of easel paintings, mostly due to photo- and thermal oxidation, produces yellowing of the varnish layer and, under specific climatic and pollution conditions, drastic changes of the mechanical properties of the painted layer and the supporting materials. Oxidation alters the appearance and readability of the painting and also contributes to the degradation of the surface by favoring the cracking of the varnish protective film.[1−4] Moreover, in the case of canvas paintings, acids produced by aging of varnish and drying oil favor additional degradation on the cellulose fibers of the canvas, through an acid-catalyzed depolymerization reaction.[5,6]

For all these reasons, aged canvas paintings usually present, together with aesthetic alterations of varnishes, great damage on the support that can eventually evolve up to laceration and rupture.

When the support is too weak to bear mechanical stress, conservators proceed with a "relining" (or lining) treatment. This procedure consists on the application of a new canvas on the back side of the paint by using synthetic adhesives or natural glues. Unfortunately, both synthetic and natural adhesives, used in the last decades for the lining procedure, have been shown to undergo severe natural aging, and it has been hypothesized that their alteration favors further degradation of the support due to the newly formed degradation products.[7] For this reason, great efforts have been recently made to detach the old lining canvas and completely remove the aged adhesives used for lining. This can be achieved by using detergent solutions and, in some cases, mixtures

Received: November 13, 2011
Revised: January 23, 2012
Published: January 24, 2012

   dx.doi.org/10.1021/la2044619 | *Langmuir* 2012, 28, 3952−3961

or pure solvents. Natural glues, such as animal glue, can also be removed from textiles using enzymes (e.g., protease).[8]

It has been recently shown that "swollen micellar solutions" and/or oil-in-water (o/w) microemulsions are greatly effective in the solubilization and removal of several polymers[9−14] from wall paintings. The ability of these dispersed systems to solubilize synthetic resins such as acrylate/methacrylate and acrylate/vinyl acetate copolymers, that are widely used in artworks conservation, makes them potentially suitable for the removal of adhesives from the backside of lined canvas and possibly for the cleaning of the painting surface (both on canvas and wood artworks).

Unfortunately, the usage of a water-based system could represent a problem during the application, because canvas easily absorbs water that can swell the preparation layer, inducing additional mechanical stress to the painting layer, often leading to the painting detachment.

The control of solvent's action is indeed a relevant topic in conservation science, as it extends to different solvents with characteristic polarity and cleaning properties. Gel technology is widely used in the field of cultural heritage conservation to prevent the penetration of solvents and/or aqueous detergent solutions into the painting layer. Wolbers has proposed the usage of several systems mainly based on water and solvents in a gelled state,[15,16] usually referred as solvent gels. Solvent gels are physical gels, typically obtained by using poly(acrylic acid) (e.g., Carbopol polymers) as gelling material, where weak attractive intermolecular forces (i.e., dipole−dipole interactions and/or hydrogen bonding) sustain the gel network. Using Wolbers' systems, the capillary penetration of the detergent system and the spreading of undesired materials into the painting layer may be mostly overcome. Moreover, the confinement into the gel reduces the solvent evaporation. Solvent gels are typically made with either nonpolar (aliphatic and aromatic hydrocarbons) or more polar organic solvents (alcohols, acetone, dimethyl sulfoxide) and are used for the cleaning of waxes and natural resins. However, the solvent-gel technology has some drawbacks; it has been shown[17] that very often gel residues (mostly due to the high molecular weight components of the Carbopol gels) remain on and beneath the painted surface after the treatment. Usually, to completely remove the physical gels, an additional cleaning step with pure solvents is mandatory,[18] leading in some cases to detrimental effects on the delicate layers of the painting.[19−21] On the same principle, other physical gels have been tested for the application of various cleaning solutions. Methylcellulose gels have been used for the application of enzymatic solutions,[22,23] but they are also likely to leave residues on the artistic substrates. O/w microemulsions were loaded into agar gels for the effective removal of hydrophobic material (wax) from porous substrates.[24] Moreover, many efforts have been recently made to apply new classes of gels able to minimize the amount of residue left over the painted surfaces after cleaning.[25−32]

It has been already shown that acrylamide based gels possess very good water loading and retention properties.[33,34] These features offer them as possible systems for confining and control of aqueous fluids in the cleaning of water-sensitive substrates. Acrylamide based chemical gels are obtained by a radical polymerization of acrylamide monomer and *N*,*N*′-methylene bisacrylamide as a cross-linker, resulting in a tridimensional network formed by polymer chains bound together by covalent bonds. In general, chemical gels result as much more structured and cohesive than physical gels; their behavior is very similar to the one of a solid, and their removal from the cleaned surface is very simple and, more important, residue-free. In this regard, Bonini et al.[33] have already studied acrylamide magnetic sponges for water-based formulations, tailored for application on marble and mural artworks. These gels are particularly feasible, since they can be removed with only minimal external intervention (i.e., simply by applying an external magnetic field). Starting from these systems, acrylamide gels have been reformulated for the treatment of canvas painting surfaces, in particular for the removal of lining adhesives.

The aim of the present work was to optimize the acrylamide hydrogel capability of confining the highly effective oil in water microemulsions[12] and to test the efficacy of the optimized gel-microemulsion system in the removal of synthetic adhesives from lined canvas without leaving any gel residues.

In particular, the monomer/cross-linker concentration ratio and water percentage were tuned to optimize water retention, loading properties and the mechanical stability of the hydrogels. The magnetic nanoparticles present in the previous case[33] were not included in the present formulation to obtain an almost transparent cleaning tool.

Two new hydrogels differing each other for the mechanical properties and the internal porosity are presented in this paper. Water retention and loading properties have been characterized by dehydration curves and free water index (FWI). Scanning electron microscopy (SEM) and small angle X-ray scattering (SAXS) have been used to extract information on the micro- and nanostructure of the hydrogels and the corresponding xerogels. Finally, the two hydrogels were loaded with a water based "swollen micellar solution"[12] effective in removing acrylic and vinyl polymers, and cleaning tests were performed on canvas replicas that had been previously treated with a widely used synthetic lining adhesive, in order to simulate lined paintings. The effect of the hydrogel confinement on the "swollen micellar" system has been investigated by SAXS.

EXPERIMENTAL SECTION

Materials. For the preparation of the gels, acrylamide (assay ≥ 99%), *N*,*N*′ methylene-bisacrylamide (assay ≥ 98%), and *N*,*N*,*N*′,*N*′-tetramethylethylene-diamine (TEMED) (purity ≥ 99%) were obtained from Fluka, Milan; ammonium persulfate (APS) (purity >98%) from Sigma-Aldrich, Milan. Sodium dodecyl sulfate (SDS) (assay ≈ 95%), propylene carbonate (PC) (purity ≥ 99%), and ethyl-acetate (EA) (purity ≥ 99.5%) were obtained from Sigma-Aldrich, Milan; 1-pentanol (purity ≥ 98.5%) from Merck. All the chemicals were used as received; water was purified by using a Millipore MilliRO-6 Milli-Q gradient system (resistance >18 MΩ·cm).

Gel Preparation. Hydrogels were obtained by a free radical copolymerization of acrylamide monomer, and a cross-linker, *N*,*N*′-methylene-bisacrylamide, in water solution. Two systems with interesting macroscopic features were selected among a library of acrylamide hydrogels obtained varying the monomer/cross-linker ratio and the total water percentage. In particular, the selected systems have a constant monomer/cross-linker ratio and different water percentages (see Table 1). Hereinafter, the hydrogel containing more polymer will be called Hard or shortly ***H***, while the other Soft or shortly ***S*** considering the different mechanical properties of the considered systems. Specifically, the Soft gel exhibited a more enhanced deformability when mechanical stress was applied, even by handling or moderate pressure. This feature, aimed at granting the ***S*** system an increased adhesion to textured surfaces, results in an enhancement of

dx.doi.org/10.1021/la2044619 | *Langmuir* 2012, 28, 3952−3961

Table 1. Compositions (w/w) of the Two Hydrogels, and the Water to Dry Solid (Xerogel) Ratio[a]

	Hard (*H*)	Soft (*S*)
acrylamide	5.28% (4.71%)	3.45% (3.07%)
N,*N*′-methylene bisacrylamide	0.88% (0.72%)	0.57% (0.46%)
water	93.84% (94.57%)	95.98% (96.47%)
g H_2O/g xerogel	15.2	23.9

[a]Cross-linker percentage was kept constant in respect of the monomer amount. Volume fraction of each component is reported in parentheses.

the surface wettability. Both ***H*** and ***S*** gels, however, are more rigid than the traditional gels used in restoration practice (solvent gels, cellulose ether gels).

In detail, 4 mL of the monomer/cross-linker solution was put into a plastic container (parallelepiped with a 2.5 cm × 2.5 cm base) whose dimensions defined the final shape of the hydrogel. Prior to polymerization, the solution was bubbled with nitrogen for 5 min, in order to remove any trace of dissolved oxygen that could inhibit the radical polymerization.

To initiate the reaction, 100 μL of ammoniumpersulfate (APS) water solution (with a concentration of 3.28 mM for the Hard and 2.19 mM for the Soft gel) was added to the reaction mixture, together with 50 μL of TEMED that allows the radical polymerization to take place at low temperature. The concentrations of APS solution resulted in a 1:100 APS/acrylamide molar ratio.

Polymerization reaction was completed at room temperature after 30 min. After polymerization, hydrogels were washed 10 times with 40 mL of distilled water, in order to remove any residue of unreacted monomers.

Gel Loading. Acrylamide/bisacrylamide hydrogels were loaded with a detergent system constituted by sodium dodecyl sulfate (SDS), 1-pentanol, ethyl acetate (EA), and propylene carbonate (PC) (or shortly EAPC system). This innovative system is very effective in removing acrylic and vinyl polymer resins.[12]

The composition of the EAPC system (reported as % w/w) is as follows: water 73.3%, SDS 3.7%, 1-pentanol 7%, PC 8%, and EA 8%. The loading of the EAPC into the hydrogel ***H*** (or ***S***) was achieved equilibrating the saturated gel (4 mL) into 30 mL of EAPC system for at least 12 h. This step induces a decrease in the concentration of the EAPC active products. The effect of the confinement of the EAPC system into the hydrogel has been investigated by SAXS and will be presented in the Results and Discussion section. In this particular case, the neat EAPC system used as a reference has been diluted in the very same way (30 mL EAPC + 4 mL of water) in order to take into account the dilution associated with the equilibration step.

Preparation of Canvas Samples and Cleaning Procedure. The cleaning tests were performed on model canvas samples treated with Mowilith DM5 to simulate a lined paintings. Mowilith DM5 is a widely used commercial copolymer of vinyl acetate (65%) and *n*-butyl acrylate (35%) in aqueous emulsion. Model samples were prepared by coating a canvas with the adhesive by means of a brush to achieve a coverage degree of 10−15 mg/cm^2.

Before the application, the surface of the EAPC loaded gels has been quickly dried using Whatman paper. The gel has been kept in contact with the canvas replica for about 4 h. In general, after the application, the polymeric adhesive appeared swollen and softened so that a gentle mechanical action was sufficient to detach most of the polymer from the canvas surface.

Physicochemical Characterization. The water content, expressed as weight fraction WC, in hydrogels was determined by differential thermogravimetry (DTG). These experiments were carried out with a SDT Q600 (TA Instruments) apparatus. The temperature scans were performed from 20 to 250 °C with a heating rate of 10 °C/min. The free water index (FWI) was calculated from the analysis of thermograms obtained by differential scanning calorimetry (DSC) with a Q1000 (TA Instruments) apparatus. The temperature range was from −80 to 20 °C with a rate of 0.5 °C/min; sealed stainless steel pans were used. In the case of saturated gels, only the melting peak corresponding to bulk-like water is present. The FWI values were calculated as follows:[28]

$$\mathrm{FWI} = \frac{\Delta H_{\mathrm{exp}}}{WC \times \Delta H_{\mathrm{theo}}} \quad (1)$$

where ΔH_{exp} [J/g] is the enthalpy variation during water melting determined by integration of the DSC peak at about 0 °C, and WC is the weight fraction of water in the hydrogel. ΔH_{theo} [J/g] is the theoretical value of the specific enthalpy of fusion for water (333.55 J/g).[28,35] The accuracy in the ΔH_{exp} determination was evaluated as ±0.5 J/g. From FWI values, it was also straightforward to evaluate the mass ratio between bound water and the xerogel, R_{bx}:

$$R_{\mathrm{bx}} = \frac{W_{\mathrm{w}} \times \mathrm{WC} \times (1 - \mathrm{FWI})}{W_{\mathrm{d}}} \quad (2)$$

where W_{d} is the weight of the xerogel and W_{w} is the weight of the fully hydrated gel.

DSC measurements were also performed on partially saturated samples (i.e., rehydrated xerogels where the porosity is partially filled) by using a humidity chamber at 98% relative humidity (r.h.). These samples allowed a better discrimination of the signals from the bound-freezable water (peak between −70 and −10 °C). The bound water index (BWI) can be calculated according to the following equation:[35]

$$\mathrm{BWI} = \frac{\Delta H_{\mathrm{exp}}}{\mathrm{WC} \times \Delta H_{\mathrm{bound}}} \quad (3)$$

where $\Delta H_{\mathrm{bound}}$ [J/g] is the theoretical value of the specific water fusion enthalpy at the melting temperature below 0 °C as reported in the literature.[36]

Additionally, dehydration curves were registered by monitoring the weight of a saturated gel sample kept in a humidity chamber at 55% r.h. (saturated $Ca(NO_3)_2$ solution) until a plateau value was reached. The water strongly bounded to the dehydrated gel was removed by using an oven at 110 °C for 12 h. The percentage of water contained in each hydrogel was calculated as follows:

$$\%\mathrm{water} = \frac{W_i - W_{\mathrm{d}}}{W_{\mathrm{w}}} \quad (4)$$

where W_i is the weight of the hydrogel at day i and the other parameters are the same as in eq 2.

SEM investigations were performed on the xerogels. A Cambridge Stereoscan 360 electron microscope, working at 20 kV of acceleration potential and at 25 mm as working distance, was used for the observations. A very thin slice of hydrogel was extensively freeze-dried to obtain the corresponding "xerogel" (sometimes referred as cryogel) and additionally coated with a gold layer (Agar Scientific Auto Sputter Coater) for the SEM analysis.

SAXS measurements were carried out with a HECUS SWAX-camera (Kratky) equipped with a position-sensitive detector (OED 50M) containing 1024 channels of width 54 μm. Cu Kα radiation of wavelength λ =1.542 Å was provided by a Seifert ID-3003 X-ray generator (sealed-tube type), operating at a maximum power of 2 kW. A 10 μm thick Ni filter was used to remove the Cu Kβ radiation. The sample-to-detector distance was 275 mm. The volume between the sample and the detector was kept under vacuum during the measurements to minimize scattering from the air. The Kratky camera was calibrated in the small angle region using silver behenate (d = 58.38 Å).[37] Scattering curves were obtained in the q-range between 0.01 and 0.54 Å^{-1}, assuming that q is the scattering vector, and 2θ the scattering angle ($q = 4\pi/\lambda \sin\theta$). Gel samples were places into a 1 mm demountable cell having Kapton films as windows. The temperature was set to 25 °C and was controlled by a Peltier element, with an accuracy of 0.1 °C. All scattering curves were corrected for the empty cell contribution considering the relative transmission factor. SAXS curves were iteratively desmeared using the procedure reported by Lake.[38]

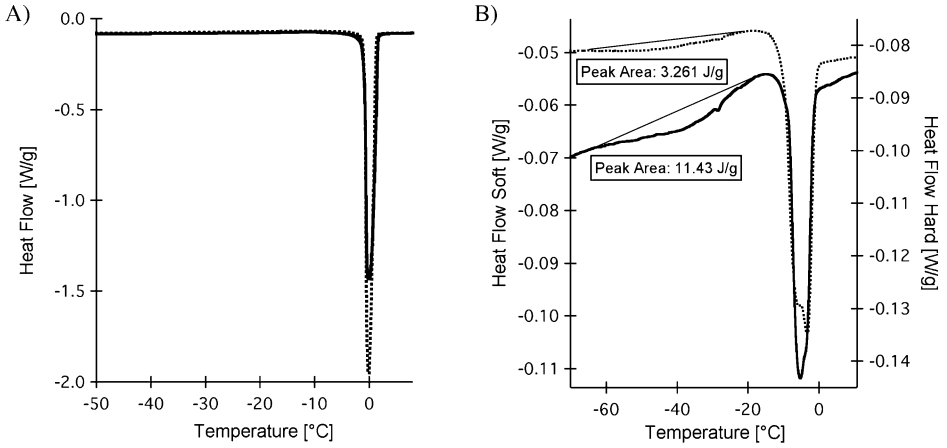

Figure 2. DSC thermograms for the Hard (solid line) and Soft (dotted line) fully hydrated gels (A) and partially rehydrated xerogels (B).

Attenuated total reflectivity (ATR) Fourier transform (FT) infrared spectroscopy was performed, with a Nexus 870 FT-IR Thermo Nicolet instrument equipped with a Golden Gate apparatus for ATR, on some canvas surfaces, previously treated with polymer resins, to detect possible gel residues remaining after cleaning tests. The cleaned canvas areas were investigated thoroughly to detect the possible presence of gel on the fibers.

RESULTS AND DISCUSSION

It is well-known[33,39] that the swelling behavior of acrylamide gels is dependent on the pH, i.e. at neutral pH the gel is more swollen than at acidic or alkaline pH. In the present work, the hydrogels were fully hydrated with water at neutral pH to achieve the maximum swollen state. After the preparation, the ***H*** and ***S*** acrylamide hydrogels were equilibrated with distilled water to achieve the maximum swelling (in about 1 week). As a result, ***S*** increased its water content from 96% to 96.5% whereas ***H*** passed from 93.8% to 94.5%.

Water in swollen hydrogels can be classified as unfreezable, bound-freezable, and free, depending on the extent of interactions with the polar portion of the polymer chains.[40] These different types of water can be determined by DSC technique: the first fraction does not freeze even at very low temperatures, the second one exhibits a freezing peak far from 0 °C, while the free water fraction exhibits the same DSC feature of bulk water.

FWI, as defined in the Experimental Section, is an important parameter that accounts for the retention properties of a hydrogel; usually the lower the FWI value, the higher is the water retention. As mentioned above, it is important to maximize the water retention inside the gel when treating hydrophilic, water-sensitive substrates, such as canvas paintings. Ideally, gels with lower FWI would prevent the uncontrolled diffusion of the loaded aqueous cleaning fluids along the plane of the canvas surface and through the cross-section of the treated porous artworks. In the context of this contribution, we characterized the different FWI for both the ***H*** and ***S*** systems and verified, through practical cleaning tests, that the gels' water retention would change accordingly. An experimental study on the quantitative correlation between the FWI/BWI parameters and water retention is beyond the scope of this study.

Figure 2 shows the DSC curves for the investigated hydrogels at two different hydration levels, and Table 2 lists the extracted FWI values. As evidenced by the FWI reported in Table 2, the majority of the water contained in the hydrogels behaves like bulk water and can be used as the continuous medium for the detergent solution that will be confined in the gel structure. R_{bx} indicates the amount of water directly or indirectly affected by the presence of the polymer network normalized to the dry weight. In the case of ***H*** gel, a slightly higher value is obtained for the fully swollen hydrogels while this difference levels off considering the rehydrated xerogels. In fact, the loss of a fraction of the original porosity induced by the freeze-drying process on the xerogels (see Figure 6B and relative explanation) minimizes the differences from the gels, and the rehydration with water vapor cannot recover the original structure. For this given reason, the detergent loading was preformed directly on the hydrogels in their swollen state (see Experimental Section).

Table 2. Free Water Index (FWI) Values and Correlated Parameters for Swollen Gels and Partially Rehydrated Xerogels (*)[a]

	ΔH_{exp} (J/g)	WC	FWI	R_{bx} (g/g)
Hard	285.0	0.946	0.903	1.68
Soft	303.5	0.961	0.947	1.33
Hard*	37.7	0.407	0.278	0.50
Soft*	47.3	0.449	0.316	0.56

[a]WC is the weight fraction of water.

Figure 2B refers to the samples obtained by xerogels rehydration with water vapor in controlled humidity conditions. DSC curves emphasize the small differences observed in FWI reported in Table 2. The thermograms highlight the presence of an extra fusion peak between −20 and −70 °C in both samples; this broad feature is commonly associated to the bound-freezable water inside the gel network. It is also evident that the ***H*** gel presented a larger signal than the ***S*** gel. The BWI linked to this additional peak was calculated according to eq 2 and is reported in Table 3.

Table 3. BWI Values and Correlated Parameters for the Partially Hydrated Gels (*) Obtained Following the Procedure Reported in the Experimental Section

	ΔH_{exp} (J/g)	BWI
Hard*	11.43	0.121
Soft*	3.26	0.033

Examples of SEM images for the Hard and Soft xerogels obtained by freeze-drying are reported in Figure 3 and 4, respectively.

dx.doi.org/10.1021/la2044619 | *Langmuir* 2012, 28, 3952−3961

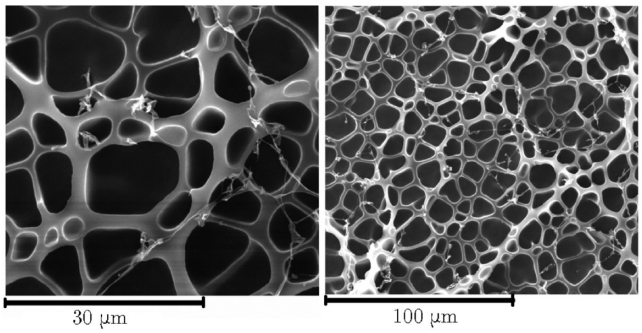

Figure 3. SEM images of Hard xerogel obtained at two different magnifications. The bright area corresponds to the acrylamide polymer while the dark area is the porosity.

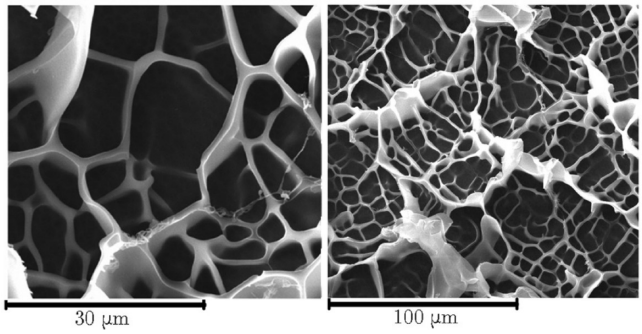

Figure 4. SEM images of Soft xerogel obtained at two different magnifications. The bright area corresponds to the acrylamide polymer while the dark area is the porosity.

A cobweb-like network morphology is present in both samples and the pore dimensions are approximately in the range from 5 to 25 μm. In the case of the ***H*** gel a more regular structure is evidenced.

Several SEM images for both xerogels have been analyzed to extract a statistical relevant pore size distribution (ImageJ software analysis[41]), and the results are reported in Figure 5.

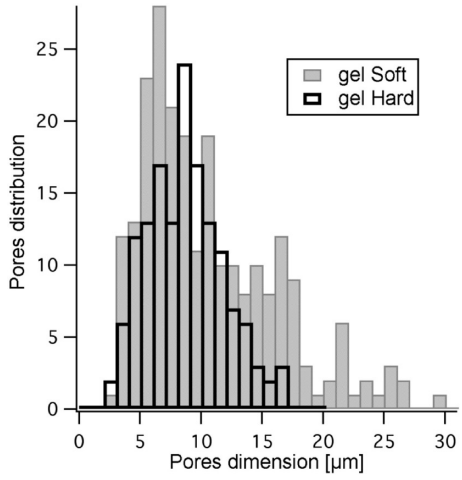

Figure 5. Pore size distributions for Hard and Soft xerogels.

As evident, in the ***S*** case a broader distribution is obtained with characteristic dimensions from 3 to 30 μm while the ***H*** case presents a thinner distribution where the maximum pore diameter is about 17 μm. The average pore sizes extracted are 10 ± 5 μm and 8 ± 3 μm in the case of ***S*** and ***H*** gel, respectively. On the contrary, the average thickness of the pore walls result slightly greater in the case of the ***H*** xerogel (1.3 ± 0.5 μm against 0.9 ± 0.3 μm) due to the higher amount of polymer used in the corresponding hydrogel formulation.

The differences in the pore size distribution and the wall thickness as well as the mechanical behavior of the two hydrogels can be linked to the volume fraction of the polymeric precursors (or on the volume fraction of water molecules) that generate the final gel porosity. Therefore, in the case of the Soft gel, a lower concentration of polymeric material (or higher percentage of water) accounts for the formation of a broader pore size distribution with thinner pores walls and weaker mechanical properties (enhanced deformability).

Figure 6 shows the SAXS curves in a log−log scale for ***H*** and ***S*** swollen hydrogels (panel A) along with corresponding xerogel cases (panel B). A power law trend is evident in the small q region for all the investigated samples either in the hydrated as well as in the freeze-dried cases. As a matter of fact, the power law exponent diminishes passing from the hydrogels (values between −2 and −3, typical of fractal-like objects) to the "xerogel" systems (values around −4 which are typical for the Porod regime of a solid with a sharp interface).

The notion of fractal applies only within two natural limits: the size of the basic unit forming the fractal, σ, and the size of the overall aggregate, δ. As the density of a fractal object changes with r^{D-3} (where r is the mean dimension of the repeating units), the scattering intensity can be written as

$$I(q) = \mathrm{A}q^{-D} \tag{5}$$

where A is a prefactor and D is the mass fractal dimension (when $1 \leq D \leq 3$). A straight line in the interval $\delta^{-1} < q < \sigma^{-1}$ of the $\log(I)$ versus $\log(q)$ plot represents a power law, and the slope of this straight line is the $-D$ exponent (see Figure 6A). The mass fractal dimension for gel ***H*** (2.77) is greater than the one extracted for gel ***S*** (2.36), or, in other words, the structure of ***H*** is denser as we could expect considering the higher polymer to water ratio used in the synthesis of the former. When the freeze-drying process is applied and the "xerogel" is obtained, the structure in the nanometric range (and the associated mesoporosity) collapses and the mass fractal is lost. In fact, both SAXS curves for the "xerogels" ***H*** and ***S*** (see Figure 6B) have an exponent of about −4, which is a typical feature of a bulk solid with a smooth interface. In this regard, the polymeric network in the "xerogel" has a characteristic dimension greater than the experimental resolution (about 50 nm) and the interface is sharp as already evidenced by the SEM investigation (see Figures 3 and 4).

In order to detail the hydrogel structure in the nanometer an analytical model must be used. According to the Debye−Bueche[42] approach, we can assume that the SAXS intensity distribution arises from two q dependent contributions and an instrumental background, bkg:

$$I(q) = I_{\mathrm{Lorentz}}(q) + I_{\mathrm{excess}}(q) + \mathrm{bkg} \tag{6}$$

In particular, the first component takes into account the scattering coming from the presence of a 3D network with a characteristic mesh size and is mathematically described as

$$I_{\mathrm{Lorentz}}(q) = \frac{I_{\mathrm{Lorentz}}(0)}{1 + q^2\zeta^2} \tag{7}$$

dx.doi.org/10.1021/la2044619 | *Langmuir* 2012, 28, 3952−3961

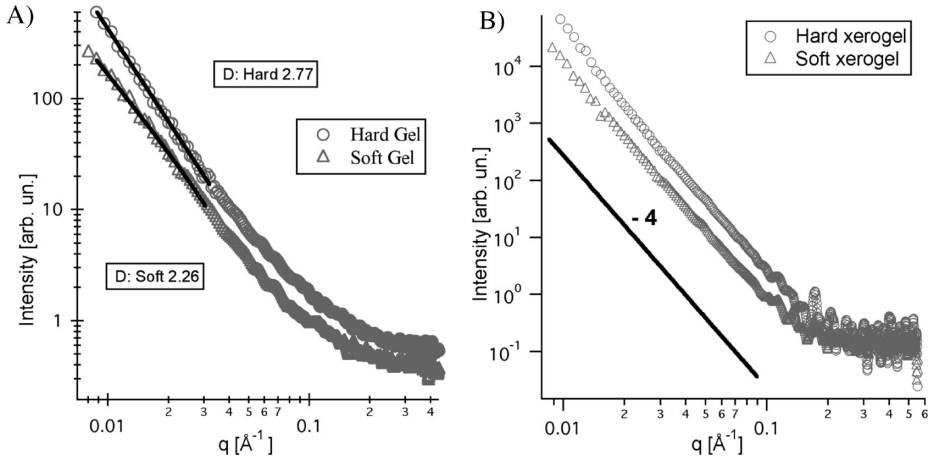

Figure 6. SAXS intensity distribution for Hard (circles) and Soft (triangles) swollen hydrogels (panel A) and "xerogels" (panel B). In panel A, the fitting of the low-q range data according to a power law is reported as a solid line for both samples. In panel B, the solid line represents a q^{-4} trend.

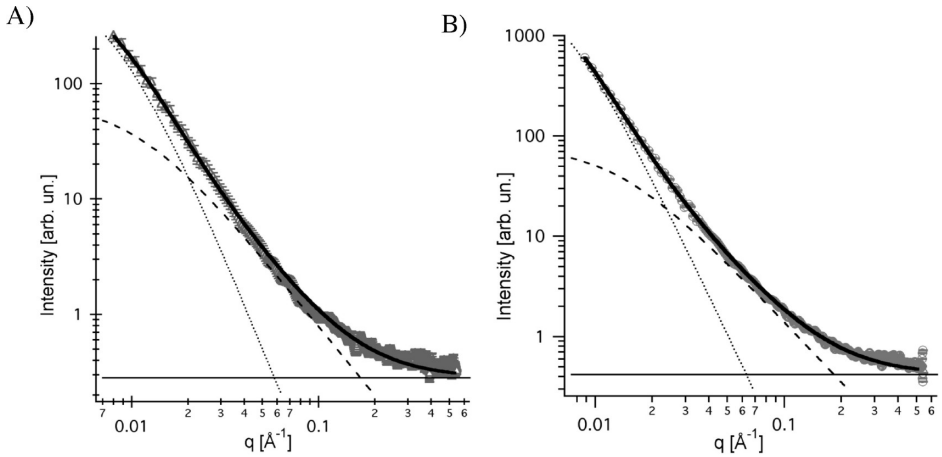

Figure 7. Debye–Bueche fitting (solid lines) of the SAXS curves of Soft (panel A), and Hard (panel B) hydrogels. The dotted and dashed lines represent the excess and the Lorentzian term, respectively. The background contribution is also reported as a continuous line parallel to the x-axis.

where $I_{\text{Lorentz}}(0)$ is the Lorentzian intensity at $q = 0$ and ζ is the average mesh size of the 3D network.

The second component, usually referred to as the excess scattering term, accounts for the low-q scattering generated from the presence of inhomogeneities[43] (i.e., solid-like polymer domains):

$$I_{\text{excess}}(q) = \frac{I_{\text{excess}}(0)}{(1 + q^2a^2)^2} \tag{8}$$

where $I_{\text{excess}}(0)$ represents the excess intensity at $q = 0$ and a is the average inhomogeneity domain size.

The experimental SAXS profiles along with the fitting curves for both hydrogels are presented in Figure 7. Table 4 lists the values of the parameters extracted by the Debye-Bueche approach.

Extracted mesh size, ζ, changes from about 7.5 to 9 nm passing from the Hard to Soft hydrogel. This small increase is strictly connected to the amount of water present in the polymerization batch since the cross-linker to monomer ratio was maintained constant for both hydrogel formulations. Concurrently, the sample with the higher polymer volume fraction (***H*** case) has a greater value of inhomogeneity dimension (17.1 nm) as compared to the ***S*** case (12.9 nm). As already reported in the literature,[44−46] this is in agreement with the tendency of the polymer network to built more heterogeneous structures in the less water-rich system. In this regard, the $I_{\text{excess}}(0)/I_{\text{Lorentz}}(0)$ ratio reveals an increase in the inhomogeneity abundance by a factor of 6 in the case of the ***H*** hydrogel. [Note: Due to the fact that SAXS measurements are not in absolute intensity, $I_{\text{excess}}(0)$ and $I_{\text{Lorentz}}(0)$ values are meaningless; however, their ratio is proportional to the ratio between inhomogeneity/mesh volume fractions.]

Table 4. Structural Parameters Obtained from the Debye–Bueche Fitting of SAXS Curves for the Hydrogels *S* and *H*

	Soft	Hard
$I_{\text{Lorentz}}(0)$	68	79
ζ (nm)	9.2 ± 1.6	7.5 ± 1.2
$I_{\text{excess}}(0)$	918	5833
a (nm)	12.9 ± 0.8	17.1 ± 0.5
background	0.28	0.42
$I_{\text{excess}}(0)/I_{\text{Lorentz}}(0)$	14	74

In order to probe the hydrogel loading properties, a SAXS investigation has been performed on both the diluted EAPC and EAPC system loaded in the ***H*** hydrogel (see the Experimental Section for the details on the loading procedure). As expected, similar results were obtained with the hydrogel ***S***

dx.doi.org/10.1021/la2044619 | *Langmuir* 2012, 28, 3952−3961

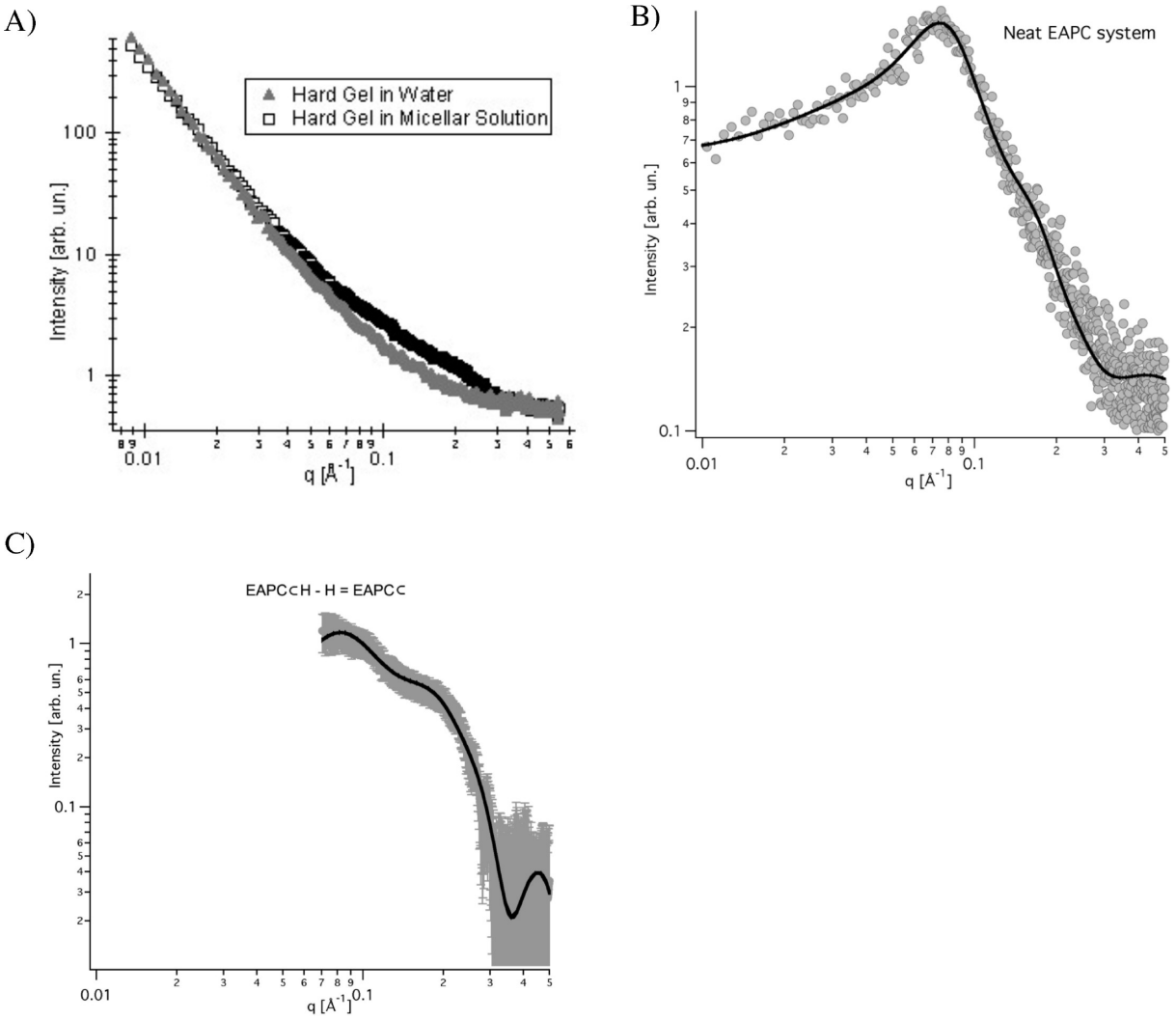

Figure 8. (A) SAXS intensity distribution for hydrogel ***H*** (full triangles) and the same hydrogel loaded by the EAPC system (empty squares). (B) SAXS intensity distribution for the neat EAPC system. (C) SAXS intensity distribution for the **EAPC⊂** system loaded in the chemical gel. Continuous lines are the best fitting obtained by the model reported in the text. In panels A and B, error bars are comparable to the data scattering and have not be included for clarity.

loaded system; for this reason, only the ***H*** case will be reported in the following discussion.

Figure 8A reports the comparison between the SAXS curves of the microemulsions loaded in the Hard gel (hereinafter labeled as **EAPC⊂*H***) and the neat Hard gel system (i.e., before the loading). The **EAPC⊂*H*** sample exhibits an excess of scattering in the q region between 0.08 and 0.25 Å^{-1}, which is roughly the same q range where the EAPC shows its maximum in the SAXS intensity (see Figure 8B). Assuming that the structure of the chemical gel is not affected by the EAPC loading and that the hydrogel contributes as a background for the EAPC scattering, the ***H*** contribution can be subtracted out from the **EAPC⊂*H*** curve to obtain the SAXS pattern of the EAPC system inside the hydrogel, **EAPC⊂** (see Figure 8C).

In a previous paper where we used a "magnetic nanosponge" as a detergent confining system, the same approach could not be applied, due to the fact that the SAXS scattering coming from the magnetic nanoparticles[33] was dominant over the scattering proper of the detergent system.

SAXS curves of neat EAPC and of EAPC systems confined in the gel network were fitted by using the NIST analysis package implemented by Kline.[47] In particular, the prolate ellipsoid model has been chosen as a form factor to describe the detergent aggregates. The model has been modified to take into account the actual volume fraction as calculated by the chemical composition and imposing a repartition percentage of the various components between the bulk and the micellar phase. A screened coulomb potential has been used to describe the interaction potential existing between the charged aggregates (structure factor). The detailed structural characterization of the EAPC system by means of the SANS contrast variation technique has been the subject of a parallel investigation[48] and was useful to unambiguously determine the relative partition of the chemical components between the microemulsion and the bulk phase (SDS 100% w/w, 1-pentanol 90%, EA 70%, PC 30%, and 7 water molecules per one SDS polar head). In the case of the **EAPC⊂**, these values were allowed to vary to take into account the interaction of the solvents with the polymer network (SDS 100% w/w, 1-pentanol 88%, EA 65%, PC 25%, and 6 water molecules per one SDS polar head).

It is important to note that the fitting procedure in the case of EAPC inside the ***H*** gel was applied only for the q range above 0.07 Å^{-1}. In fact, the points below 0.07 Å^{-1} present an error percentage that renders the data meaningless.

dx.doi.org/10.1021/la2044619 | *Langmuir* 2012, 28, 3952−3961

Table 5 reports the results of the fitting for both systems. The decrease of the major semiaxis, *a*, is related to the changed

Table 5. Structural Parameters Obtained from the Fitting of SAXS Curves for the Neat EAPC System and the EAPC System Loaded Inside the Gel *H* (EAPC⊂)

	neat EAPC	EAPC⊂
a (Å)	92 ± 4	75 ± 5
b (Å)	15 ± 1	16 ± 1
charge	5.0 ± 0.4	7.8 ± 1
volume fraction	0.206	0.194

compositional parameters. In fact, the small percentage of organic solvents that migrates out of the microemulsion droplets when they are surrounded by the gel network causes a decrease in the volume fraction of the scattering objects and a rearrangement of the microemulsion structure. The change in volume fraction strictly reflects the change in the ellipsoidal volume, meaning that the number density of the system remains constant. Moreover, the presence of a dipolar polymer, like acrylamide gels, induces a change in the charge of the micelles as emphasized by the two different fitting.

An in depth SANS investigation on the hydrogenated EAPC/D_2O system loaded in the perdeuterated hydrogel will be the straightforward confirmation of the proposed picture. It is worth to note that, on a very similar system,[33] the original microemulsion could be reobtained simply by squeezing the loaded acrylamide gel as a confirmation that the uptake/release process is reversible and that the presented hydrogels can be used for several cleaning cycles until the mechanical properties are retained.

Application of Gels. In order to assess the hydrogel behavior during the application tests, the dehydration curves have been monitored, as reported in Figure 9. The systems

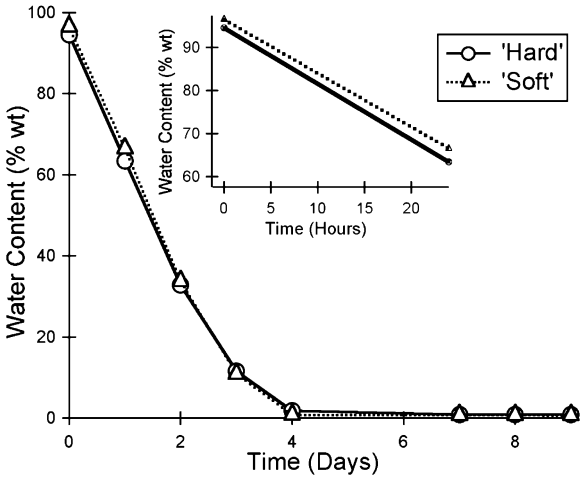

Figure 9. Dehydration curves for ***H*** (circles) and ***S*** (triangles) hydrogels. Inset: dehydration curves within 1 day of application.

behave similarly, and in about 4 days the water has been released almost completely (WC reaches 0.8% for ***S*** and 1.9% for ***H***). On the other hand, within few hours (the time requested by the cleaning test), the water retained in the hydrogel is still more than 90% (see inset of Figure 9), making these two formulations ideal as confining tools for detergent system.

Figure 10 shows the gels during the application test. It is evident that hydrogel ***S*** releases part of the liquid phase even

Figure 10. ***S*** gel (on the left) and ***H*** gel (on the right) during a cleaning application.

outside the application area, along the plane of canvas surface (see left panel of Figure 10), while hydrogel ***H*** performs the cleaning effect only in the contact area with the canvas. The significantly different applicative behaviors of the two systems correlate with the thermodynamic parameters highlighted by investigation through DSC. The lower FWI and the higher R_{bx} values found for the ***H*** gel are in agreement with the higher water retention that this system shows with respect to its "softer" equivalent. Moreover, as far as the SAXS analysis proved that the gels' mesoporosity is dramatically altered in the freeze-drying process, the higher BWI value exhibited by partially hydrated ***H*** xerogels is also consistent with the retention difference. The performances of the two gels can also be ascribed to their different macrostructures and porosities as highlighted in SEM images (and relative discussion). On this regard, SAXS investigation has shown a more compact structure and a smaller polymer mesh size in the case of the more concentrated system, ***H***. For these given reasons, we can state that hydrogel ***S*** is a worse system than ***H*** for the water-sensitive materials like canvas paintings.

Hydrogel ***H***, in this particular application, represents a good compromise between water retention and cleaning power. The SAXS measurements highlighted that both the structural parameters and the composition of the EAPC system changed only to a minimal extent due to loading inside the gel, but its number density remained unaltered, allowing the effective swelling of the lining adhesive.

Figure 11 shows the cleaning results after the application of gel ***H*** and a gentle mechanical action. The cleaned area is better visualized with SEM; the image is reported in Figure 12.

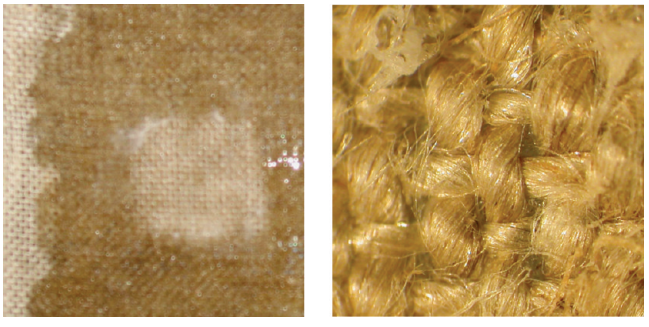

Figure 11. Result of the cleaning test: (A) image of the cleaned area; (B) microscopy magnification (×10) of the same area.

dx.doi.org/10.1021/la2044619 | *Langmuir* 2012, 28, 3952−3961

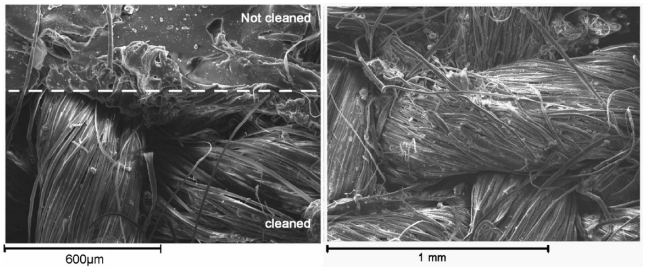

Figure 12. SEM images of the cleaned canvas. In the left panel the border between the cleaned and not cleaned area is highlighted.

All these images highlight the good cleaning action performed by the proposed formulation. The canvas resulted cleaned on the surface even tough inside the meshes of yarn some adhesive residues are still present. This cleaning result is a good starting point, since the **EAPC⊂H** system was able to swell and soften the adhesive without water spreading, hence perfectly localizing the detergent action. It is worth noticing that these results, obtained on laboratory model samples, add to previous cleaning tests, performed using nanostructured fluids loaded in our gels. These experiments were carried out with good results on canvas samples coated with aged adhesives.[7] Thermal and hydrothermal aging were considered to simulate natural aging processes.[7,49]

On the extent of confirming the absence of gel residues after the cleaning step, a supplementary test has been performed. A canvas was treated with the Hard gel loaded only with water. After 4 h of application, the gel was removed and the canvas was dried. ATR-IR spectra were collected on different spots, in order to thoroughly investigate the cleaned area. Figure 13

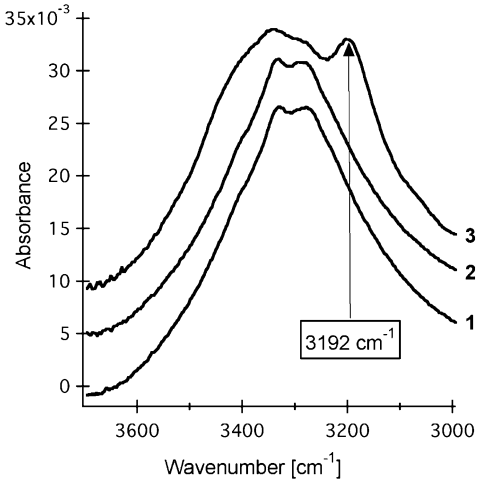

Figure 13. ATR−IR spectra of H gel (3), canvas before application (1), and canvas after application (2). An arbitrary offset has been applied to increase the readability of the graph.

shows representative ATR-IR spectra of the treated and not treated canvas, compared with the spectrum of dried gel, in the 3000−3700 cm^{-1} region. The canvas' spectra before and after the application are very similar in the whole spectral region. In particular, the peak at 3192 cm^{-1} (due to the symmetric stretching of NH_2), which is typical of the acrylamide polymer,[50] is not detected in the treated canvas spectrum. The presented result confirms that acrylamide chemical gels do not leave any detectable residue on the treated surfaces.

CONCLUSIONS

In this paper, we reported the synthesis and the characterization of two acrylamide gels having different polymer network concentrations and retaining a constant cross-linker/monomer ratio. This compositional difference affects the macroscopic characteristic (mechanical properties) and application behavior of the presented hydrogels. The physicochemical characterization has been focused on the comprehension and explanation of these differences. The correlation between thermodynamic analysis, nanostructural characterization (SAXS), and the macroscopic behavior of gels in relevant applications concurred in shedding new light on promising materials that had proven to be effective in the Cultural Heritage conservation,[25,29,33] improving the understanding of their cleaning and applicative mechanisms.

Both hydrogels exhibit highly porous interconnected structures, but, as a matter of fact, a higher concentration of polymer produces a more compact gel structure where water is trapped in a smaller mean pore size and thicker pore walls. This evidence can explain the different mechanical properties and water retention capacity of the two systems.

SAXS analysis reveals that the nanodroplets of solvents and surfactant can be included inside the gel structure, creating a useful system for the cleaning of works of art. The capability to support innovative and environmental friendly aqueous cleaning fluids, whose effectiveness toward detrimental coatings had been previously proved,[7,12] while also controlling their diffusion on water-sensitive substrates, are indeed significant advances, pointing to new applications of nanotechnology to conservation science.

Moreover, the lack of detectable gel residues on the cleaned surface represents a crucial factor that offers these systems as a real alternative to the widely used solvent gels.[17]

AUTHOR INFORMATION

Corresponding Author

*Telephone: +39 055 457-3033. Fax: +39 055 457-3032. E-mail: baglioni@csgi.unifi.it. URL: www.csgi.unifi.it.

Notes

The authors declare no competing financial interest.

ACKNOWLEDGMENTS

Thanks are due to Dr. F. Ridi for the help with thermal analysis experiments and to Dr. M. C. Arroyo for ATR-IR measurements. Financial support from Ministero dell'Istruzione, dell'Università e della Ricerca Scientifica (MIUR, Grant PRIN-2008, prot. 20087K9A2J) and Consorzio Interuniversitario per lo sviluppo dei Sistemi a Grande Interfase (CSGI) is gratefully acknowledged.

REFERENCES

(1) Pastorova, I.; van der Berg, K. J.; Boon, J. J.; Verhoeven, J. W. *J. Anal. Appl. Pyrolysis* **1997**, *43*, 41−57.
(2) Marengo, E.; Liparota, M. C.; Robotti, E.; Bobba, M. *Vib. Spectrosc.* **2006**, *40*, 225−234.
(3) Van der Doelen, G. A.; Boon, J. J. *J. Photochem. Photobiol., A* **2000**, *134*, 45−57.
(4) De la Rie, E. R. *Stud. Conserv.* **1988**, *33*, 53−70.
(5) Seves, A. M.; Sora, S.; Scicolone, G.; Testa, G.; Bonfatti, A. M.; Rossi, E.; Seves, A. *J. Cultural Heritage* **2000**, *1* (3), 315−322.
(6) Testa, G.; Sardella, A.; Rossi, E.; Bozzi, C.; Seves, A. *Acta Polym.* **1994**, *45*, 47−49.

(7) Chevalier, A.; Chelazzi, D.; Baglioni, P.; Giorgi, R.; Carretti, E.; Stuke, M.; Menu, M.; Duchamp, R. *Proceedings of the "ICOM-CC 15th Triennial Conference, 22−26 September 2008, New Delhi (India)"*, 2008; Vol. 2, pp. 581−589.
(8) Ahmed, H. E.; Kolisis, F. N. *J. Appl. Polym. Sci.*, published online Nov 22, 2011, DOI: 10.1002/app.34053.
(9) Carretti, E.; Dei, L.; Baglioni, P. *Langmuir* **2003**, *19*, 7867−7872.
(10) Carretti, E.; Fratini, E.; Berti, D.; Dei, L.; Baglioni, P. *Angew. Chem., Int. Ed.* **2009**, *48*, 8966−969.
(11) Carretti, E.; Giorgi, R.; Berti, D.; Baglioni, P. *Langmuir* **2007**, *23*, 6396−6403.
(12) Giorgi, R.; Baglioni, M.; Berti, D.; Baglioni, P. *Acc. Chem. Res.* **2010**, *43*, 695−704.
(13) Baglioni, M.; Rengstl, D.; Berti, D.; Bonini, M.; Giorgi, R.; Baglioni, P. *Nanoscale* **2010**, *2*, 1723−1732.
(14) Baglioni, M.; Giorgi, R.; Berti, D.; Baglioni, P. *Nanoscale* **2012**, *4* (1), 42−53.
(15) Wolbers, R. *Workshop on new Methods in the Cleaning of Paintings*; Getty Trust Publications: Marina del Rey, 1988.
(16) Wolbers, R. *Cleaning Painted Surfaces: Acqueos Methods*; Archetype Publication Ltd: London, 2000.
(17) Stulik, D.; Miller, D.; Khamjian, H.; Khandekar, N.; Wolbers, R.; Carlson, J.; Petersen, W. C.; Dorge, V. *Solvent Gels for the Cleaning of Works of Art: The Residue Question*; Getty Trust Publications: Marina del Rey, 2004.
(18) Stravroudis, C.; Blank, S. *WAAC Newsl.* **1989**, *11* (2), 2−10.
(19) Burnstock, A.; Kieslich, T. *11th Triennial Meeting, Edinburgh, 1−6 September 1996, Preprints: ICOM Committee for Conservation*; Bridgland, J., Ed.; Maney Publishing: London, 1996.
(20) Burnstock, A.; White R. *Conservation Science in the U.K.: Preprints of the Meeting Held in Glasgow*; Tennent, N. H., Ed.; James & James Science Publishers: London, 1993.
(21) Burnstock, A.; White R. *Cleaning, Retouching and Coatings: Technology and Practice for Easel Paintigs and Polychrome Sculture: Preprints of the Contributions to the Brussels Congress*; Mills, J. S.; Smith, P., Eds.; London, 1990.
(22) Hatton., M. *The Paper Conservator* **1977**, *2*, 9.
(23) Blüher, A.; Banik, G.; Maurer, K. H.; Thobois, E. *Proceedings of the "ICOM-CC 11th Triennial Meeting, 1−6 september 1996, Edinburgh"*, 1996; pp. 494−499.
(24) Gorel, F. *CeROArt* **2010**, published online (http://ceroart.revues.org/1827).
(25) Baglioni, P.; Dei, L.; Carretti, E.; Giorgi, R. *Langmuir* **2009**, *25*, 8373−8374.
(26) Carretti, E.; Dei, L.; Weiss, R. G. *Soft Matter* **2005**, *1*, 17−22.
(27) Carretti, E.; Dei, L.; Baglioni, P.; Weiss, R. G. *J. Am. Chem. Soc.* **2003**, *125*, 5121−5129.
(28) Carretti, E.; Grassi, S.; Cossalter, M.; Natali, I.; Caminati, G.; Weiss, R. G.; Baglioni, P.; Dei, L. *Langmuir* **2009**, *25*, 8656−8662.
(29) Carretti, E.; Bonini, M.; Dei, L.; Berrie, B. H.; Angelova, L.; Baglioni, P.; Weiss, R. G. *Acc. Chem. Res.* **2010**, *43*, 751−760.
(30) Natali, I.; Carretti, E.; Angelova, L.; Baglioni, P.; Weiss, R. G.; Dei, L. *Langmuir* **2011**, *27* (21), 13226−13235.
(31) Angelova, L.; Terech, P.; Natali, I.; Dei, L.; Carretti, E.; Weiss, R. G. *Langmuir* **2011**, *27*, 11671−11682.
(32) Bonini, M.; Lenz, S.; Giorgi, R.; Baglioni, P. *Langmuir* **2007**, *23*, 8681−8685.
(33) Bonini, M.; Lenz, S.; Falletta, E.; Ridi, F.; Carretti, E.; Fratini, E.; Wiedenmann, A.; Baglioni, P. *Langmuir* **2008**, *24*, 12644−12650.
(34) Kizilay, M. Y.; Okay, O. *Polymer* **2004**, *45*, 2567−2576.
(35) Wenbo, L.; Feng, X.; Rongshi., C. *Front. Chem. China* **2007**, *2*, 188−192.
(36) Grant, S. A.; Sletten, R. S. *Environ. Geol.* **2002**, *42*, 130−136.
(37) Blanton, T.; Huang, T. C.; Toraya, H.; Hubbard, C. R.; Robie, S. B.; Louer, D.; Gobel, H. E.; Will, G.; Gilles, R.; Raftery, T. *Powder Diffr.* **1995**, *10*, 91−95.
(38) Lake, J. A. *Acta Crystallogr.* **1967**, *23*, 191−194.
(39) Gemeinhart, R. A.; Guo, C. In *Reflexive Polymers and Hydrogels*; CRC Press, LLC: Boca Raton, FL, 2004; pp 245−257.
(40) Wolfe, J.; Bryant, G.; Koster, K. L. *CryoLetters* **2002**, *23*, 157−166.
(41) Abramoff, M. D.; Magelhaes, P. J.; Ram, S. J. *Biophotonics Int.* **2004**, *11*, 36−42.
(42) Debye, P.; Bueche, A. M. *J. Appl. Phys.* **1949**, *20*, 518−525.
(43) Vesperinas, A.; Eastoe, J.; Wyatt, P.; Grillo, I.; Heenan, R. K. *Chem. Commun.* **2006**, *42*, 4407−4409.
(44) Ikkai, F.; Shibayama, M. *J. Polym. Sci., Part B: Polym. Phys.* **2005**, *43*, 617−628.
(45) Panyukov, S.; Rabin, Y. *Phys. Rep.* **1996**, *269*, 1−131.
(46) Benguigui, L.; Boue, F. *Eur. Phys. J. B* **1999**, *11*, 439−444.
(47) Kline, S. R. *J. Appl. Crystallogr.* **2006**, *39*, 895−900.
(48) Baglioni, M; Berti, D.; Giorgi R.; Baglioni P. Manuscript in preparation.
(49) Chelazzi, D.; Chevalier, A.; Pizzorusso, G.; Giorgi, R.; Menu, M.; Baglioni, P. Manuscript in preparation.
(50) Murgan, R.; Mohan, S.; Bigotto, A. *J. Korean Phys. Soc.* **1998**, *32*, 505−512.